



# Coalescence kinetics of unequal sized nanoparticles

T. Hawa<sup>a, b</sup>, M.R. Zachariah<sup>a, b, \*</sup>

<sup>a</sup>*Department of Mechanical Engineering and Department of Chemistry and Biochemistry, University of Maryland, College Park, MD, USA*

<sup>b</sup>*National Institute of Standards and Technology, Gaithersburg, MD, USA*

Received 3 August 2004; received in revised form 16 February 2005; accepted 24 February 2005

## Abstract

The largest collision kernel is between a small particle with high mobility, and a larger particle which presents a large collision cross-section. However, most coalescence models are limited to the analysis of equivalent particle sizes. In this paper we focus on understanding the coalescence mechanisms of unequal sized nanoparticles. We have studied the coalescence of pairs of silicon nanoparticles of volume ratios between 0.053 and 1 with 10 000 (at 1500 K) and 1600 (at 1000 K) silicon atoms using molecular dynamics (MD) simulation under constant temperature conditions. We found that the convection processes, and deformation of the smaller particle dominated the coalescence process for liquid-like particles. On the other hand, for near solid-like particles diffusion processes dominated the coalescence of nanoparticles. Coalescence processes become faster when the ratio of two particle sizes (smaller/larger) approaches zero. Most importantly we find that the Koch–Friedlander (KF) accurately predicts the coalescence time of two unequal sized particles when benchmarked against the MD simulation results, and that the characteristic coalescence times is independent of the volume ratio of the coalescing partners.

© 2005 Elsevier Ltd. All rights reserved.

*Keywords:* Sintering; Coagulation; Coalescence; Molecular dynamics; Nanocrystals

## 1. Introduction

Nanoparticles and nanocrystals of characteristic length less than 10 nm can show electronic and transport properties different from the bulk, resulting from quantum confinement and surface states (Colvin, Alivisatos, & Tobin, 1991; Goldstein, Echer, & Alivisatos, 1992; Alivisatos, 1996; Shi, Gider, Babcock,

\* Corresponding author. Department of Mechanical Engineering and Department of Chemistry and Biochemistry, University of Maryland, College Park, MD, USA. Tel.: +1 301 405 4311; fax: +1 301 314 9477.

*E-mail address:* [mrz@umd.edu](mailto:mrz@umd.edu) (M.R. Zachariah).

& Awschalom, 1996). Nanoparticles and nanocrystals have been shown to be quite useful as the building blocks to structural materials (Helble & Sarofim, 1989; Barnes, Mahurin, Mehta, Sumpter, & Noid, 2002). These imply that controlling particle size during the manufacturing process is key to the utilization of these properties.

Synthesis methods for near monodisperse colloidal particles have been developed in the liquid phase, which employ solvation forces to retard and control cluster–cluster interactions (Matijevic, 1985, 1986). However, purities of those particles are unknown, and the investigation of surface passivation effects are not fully understood (Grieve, Mulvaney, & Grieser, 2000; Murray, Kagan, & Bawendi, 2000; Trindade, O'Brien, & Pickett, 2001). On the other hand, gas-phase processes are generally cleaner than liquid-phase processes, the latter requiring the removal of solvents and other products of synthesis (Kruis, Fissan, & Peled, 1998). Moreover, the economics of vapor-phase particle production is generally more favorable than liquid phase processes and is the primary reason that most industrial scale production is done in the aerosol phase. Given the industrial relevance of the latter mechanism it is important to understand the rate controlling parameters in the coagulation/coalescence of particles in the aerosol phase.

To study the mechanisms of the nanoparticles formation in gas phase after nucleation, one needs to focus on coagulation process, where the size of the spherical primary particles and the growth of agglomerates are determined by the rate of collision and subsequent coalescence. Qualitatively, at sufficiently high temperature, particles coalesce faster than they collide, and collisions of particles will result in a spherical large particle. However, at lower temperature, particle coalescence is negligibly slow, and a collection of smaller attached particles (aggregates) is produced.

$$\tau_{\text{coalescence}} < \tau_{\text{collision}} \rightarrow \text{Spherical particle,}$$

$$\tau_{\text{coalescence}} > \tau_{\text{collision}} \rightarrow \text{Agglomerate.}$$

Thus, an understanding of the collision and coalescence is essential for desired particle morphology and size.

The formation mechanisms of nanoparticles coalescence have been studied extensively, including evaporation–condensation, viscous flow, solid state diffusion, and plastic deformation (Ulrich, 1971; Ulrich & Riehl, 1982; Bolsaitis, McCarthy, & Mohiuddin, 1987; Koch & Friedlander, 1990; Lehtinen, Windeler, & Friedlander, 1996). The linear rate law for decrease in the surface area was developed by Koch and Friedlander as

$$\frac{da}{dt} = -\frac{1}{\tau_f}(a - a_{\text{sph}}), \quad (1)$$

where  $a$  is surface area of particles,  $a_{\text{sph}}$  is surface area of sphere of same volume, and  $\tau_f$  is characteristic coalescence time. For bare particles of the characteristic coalescence time calculated from a solid-state diffusion model is written as (Friedlander & Wu, 1994)

$$\tau_f = \frac{3kT_p N}{64\pi\sigma D}, \quad (2)$$

where  $T_p$  is the particle temperature,  $N$  is the number of atoms in the particle,  $D$  is the diffusion coefficient reported as an Arrhenius function of the temperature, and  $\sigma$  is the surface tension. For droplets of equivalent sizes, the coalescence time is given by (Frenkel, 1945)

$$\tau_f = \frac{\eta d_p}{\sigma}, \quad (3)$$

where  $d_p$  is the diameter of the particle and  $\eta$  is the temperature dependent viscosity. In a prior molecular dynamics (MD) study of the kinetics of growth and coalescence of silicon nanoparticles we found that Eqs. (2) and (3) provide a reasonable quantitative description of nanoparticles coalescence (Zachariah & Carrier, 1999).

However, all sintering models accounting for particle growth by coagulation and sintering in the free molecular regime assume that aggregates collide as spherical particles of equal volume. On the other hand the largest collision kernel is between a small particle with high mobility, and a larger particle which presents a large collision cross-section (Seinfeld & Pandis, 1998). Obviously then, the most important coalescence event is also between a small and a large particle, and is the focus of this paper.

Because the coalescence process generally involves large deformations in three dimensions with a free surface, previous investigations are limited mostly to simple observational experiments (Ryley & Bennett-Cowell, 1967; Spengler & Gokhale, 1973; Park & Blair, 1975; Bradley & Stow, 1978; Ashgriz & Poo, 1990; Jiang, Umemura, & Law, 1992; Orme, 1997), highly simplified theoretical studies (Frenkel, 1945; Mackenzie & Shuttleworth, 1949; Sherer, 1977), and a limited number of computational studies (Foote, 1975; Ashgriz & Poo, 1991; Martinez-Herrera & Derby, 1995; Menchaca-Rocha et al., 1997; Nobari, Jan, & Tryggvason, 1996; Zhou & Derby, 1998). Recently, a Galerkin finite element method in conjunction with the spine-flux method for the free surface tracking was used to study the effect of Reynolds number, drop size ratio, impact velocity, and internal circulation on the collision/coalescence of dissimilar large drops (Mashayek, Ashgriz, Minkowycz, & Shotorban, 2003). During the initial stages of coalescence of unequal sized drops, large deformations in the smaller drop were observed. More recently, a computationally efficient model for the coalescence of both equal and unequal sized particles was presented using a modified Hippopede curve, to approximate the fluid surface of the coalescing particles (Garabedian & Helble, 2001; Yadha & Helble, 2004). They found that shrinkage lengths, and surface areas, were in good agreement with results reported from finite element calculations (Martinez-Herrera & Derby, 1995) but that these coalescence times did not scale linearly with either, the particle size ratio, or the total mass of the particle system.

MD simulations have been employed to study the coalescence of equal sized nanoparticles (Zhu & Averbach, 1996; Lewis, Jensen, & Barrat, 1997; Raut, Bhagat, & Fichthorn, 1998; Zachariah & Carrier, 1999; Hendy, Brown, & Hyslop, 2003). While Zeng, Zajac, Clapp, and Rifkin (1998) studied the coalescence of unequal sized nanofibers using MD simulations, and found that the smaller fiber became amorphous and exhibited accelerated bulk diffusion, to the best of our knowledge, studies of the effect of drop or fiber size ratios on coalescence processes are limited, and there is no work that investigated the effect of particles size ratios on the coalescence of nanoparticles.

In this paper we focus on understanding the coalescence mechanisms of unequal sized nanoparticles. We use classical MD simulations using the Stillinger–Weber (SW) potential (Stillinger & Weber, 1985) for the silicon system to track the evolution of the coalescence process and to obtain the coalescence time. We clarify the relationship for dynamics of coalescence of unequal sized particles, and provide insight into the relationship between the MD simulation and the Koch–Friedlander (KF) model.

## 2. Phenomenological model

Eqs. (2), (solids) and (3), (liquids) have been widely applied to estimate the characteristic coalescence time for two equivalent spherical particles. Recently, the effect of particle sizes on the melting point and

corresponding rate of nanoparticles coalescence was considered [Xing and Rosner \(1999\)](#). They reported that their model, extended from Eq. (2), satisfactorily described experimental data on Al<sub>2</sub>O<sub>3</sub> and TiO<sub>2</sub> particle formation and that the coalescence rate is very sensitive to particle size.

In a prior work we conducted MD simulations of equal sized silicon particles, and showed that the MD results compared well with the usual sintering kinetics models for both liquids and solids ([Zachariah & Carrier, 1999](#)). More recently, we have investigated surface (hydrogen) passivation on the sintering and morphology of silicon nanoparticles using MD simulations, and presented a mathematical model to describe the dynamics during the coalescence of the coated particles ([Hawa & Zachariah, 2004a,b,2005](#)). Our model, extended from Eq. (3), was able to describe the entire coalescence process, which contained both an initial induction, and the nominal coalescence periods, and was found to agree with our MD results. The model introduced the concept of an effective surface tension, which approached the true surface tension at very low surface coverage. With increasing coverage, the effective surface tension decreases, making it harder for particles to coalesce.

Here we consider the application of the KF model (1) with characteristic coalescence times described by Eqs. (2) and (3) to the coalescence of unequal sized particles. In looking at the models (2) and (3) it is clear that surface properties play an important role in the coalescence event. The driving force for coalescence is the minimization of the surface free energy, through the surface tension parameter. This naturally begs the question as to the constancy of surface tension as a function of particle size. We have found that for covalently bonded structures, where bonding is highly directional, that surface curvature effects are not sufficient to significantly alter either bond lengths or angles, with the result that surface tension was found to be particle size independent ([Schweigert, Lehtinen, Carrier, & Zachariah, 2002](#); [Hawa & Zachariah, 2004b](#)). The result is that to first order, surface tension can be regarded as a constant.

The diffusion coefficient and viscosity are obviously important in both the solid-state and the liquid-state coalescence events. At the microscopic level, coalescence is essentially an atomic diffusion process. According to the analysis mentioned above, the surface diffusion coefficient depends on curvature of the particle surface ([Xing & Rosner, 1999](#)). However, based on prior MD calculations where we did not see a significant size-dependant diffusion coefficient for silicon, we use it as a fixed parameter in our phenomenological model ([Zachariah, Carrier, & Blaisten-Barojas, 1996](#)).

During coalescence, the formation of new chemical bonds between the atoms decreases the potential energy of the system, and decreases the total surface area. For two isolated particles under adiabatic conditions, by conservation of energy, the decrease in potential energy causes a rise in the kinetic energy of atoms in the particle, which is reflected as an increase in particle temperature ([Zachariah & Carrier, 1999](#)). The temperature change of clusters affects properties such as diffusivity and complicates the calculation of characteristic coalescence time from Eqs. (2) and (3). In order to simplify this problem we chose to study the coalescence process under constant temperature conditions. In point of fact for a real growth process, particles of this size would not see temperature excursions, since they are effectively thermostated by surrounding gas ([Mukherjee, Sonwane, & Zachariah, 2003](#)).

Since the driving force for coalescence is a minimization of the number of dangling bonds through a decrease in surface area, the difference between the total surface area before and after coalescence is expected to be an important factor in the characteristic coalescence time. Assuming particles maintain a spherical shape before and after coalescence, the total surface area after coalescence is expressed in terms of total volume,  $V$ , as

$$a_{\text{sph}} = (36\pi V^2)^{1/3}. \quad (4)$$

The total surface area before coalescence is the summation of the surface area of the two particles, and depends on the initial volume difference.

$$a = (36\pi V^2)^{1/3} \left[ \left( \frac{1}{1+x} \right)^{2/3} + \left( \frac{x}{1+x} \right)^{2/3} \right]. \quad (5)$$

Here,  $x$  is an initial volume ratio of one particle to another. When  $x = 1$ , particles are of equal size. We note that the characteristic times in Eqs. (2) and (3) in the KF model (1) are independent of particle volume ratios.

### 3. Numerical procedure

To track coalescence we employ atomistic simulation approach using classical MD. For this study we use the SW potential for silicon developed by Stillinger and Weber (1985). Similar sets of potential energy functions have also been developed by Tersoff (1986, 1988a, b, 1989). However, the simulation of liquid silicon was not well described by the potential (Tersoff, 1988b). By contrast, the SW potential is designed to describe interactions in both solid and liquid forms of silicon. Since most synthesis processes leading to cluster formation occur at high temperature, cluster growth by coalescence is dominated by liquid-like characteristics, and the accuracy of the SW potential increases with increasing particle size or temperature, we use this potential for our investigations. The SW potential energy is a sum of two and a three-body interactions, and the details of the model and its parameters are given in the reference (Stillinger & Weber, 1985).

All simulations were run either on an Origin or Cray T3E computer running up to 64 processors. Atom trajectories were determined by integrating the classical equations of motion using the velocity form of the Verlet algorithm (Verlet, 1967), with rescaling of atomic velocities at each time step to achieve temperature control. Time steps of 0.5 fs were typically used to ensure energy conservation, and a Verlet neighbor list with parallel architecture was employed in all the simulations, with a neighbor list renewal every 10 steps. The simulations take place in a spherical cavity of 20 nm radius using an elastic boundary condition.

The first step in the equilibration process was to prepare silicon particles of various sizes (500, 1000, 2000, 3000, 4000, 5000, 6000, 7000, 8000, 9000, and 9500 Si atoms) at 2100 K. After removal of angular momentum, particle temperatures were reduced slowly to 1500 K and equilibrated for 50 ps. For the last step in the preparation process, the simulations were switched to a constant energy calculation for 20 ps. If the average temperature of the particle deviated by more than 10 K over this period, the equilibration process was repeated until the particle temperature deviated by less than 10 K. Similarly, solid particles of various sizes (160, 320, 640, 960, 1280, 1600, 1920, 2240, 2560, 2880, and 3040 Si atoms) were equilibrated at 1000 K. Sizes of solid particles were chosen to be smaller than those of liquid particles due to the expensive simulation cost for complete coalescence.

Duplicated particles were generated for both temperatures and then collided with energies equivalent to the internal temperature of the particles in order to simulate thermal collisions. In our study, all coalescence processes were executed in a constant temperature simulation. We studied the coalescence of following particle pairs: (500–9500, 1000–9000, 2000–8000, 3000–7000, and 4000–6000) for 1500 K and (80–1520, 160–1440, 320–1280, 480–1120, and 640–960) for 1000 K. After complete coalescence,

all liquid and near solid-like pairs form spherical particles (about 8 and 4 nm) containing 10 000 and 1600 Si atoms.

#### 4. Results and discussion

To understand the mechanism of two unequal sized particles coalescence, we present the temporal evolution of the silicon nanoparticles during coalescence shown as a cross-section slice in Fig. 1. The particle pair consists of 500 dark gray atoms in a smaller particle and 9500 light gray atoms in a larger particle at 1500 K. At the beginning of the simulation, two particles approach at thermal speeds and have an initial contact (a). Once the collision event has initiated, diffusion processes deform the smaller particle to increase the contact area between the two particles. The radius of the contact circle quickly grows to roughly the initial radius of the smaller particle (b). At this point the contact circle seems nearly flat, and no significant deformation is seen in the larger particle. Further reduction of surface area progress smoothly (c) as the smaller particle is stretched in the vertical direction to maximize contact area, with only a minimal deformation in the larger particle. Further smearing of the smaller particle results in an effective contact area twice that of the initial small particle diameter at the point where the overall shape is close to being spherical (d).

To better understand the nature of the evolution in the morphology, we study the properties of particles at temperatures of 1500 K (liquid) and 1000 K (near solid-like) in detail. Since the temporal change in morphology can be through bulk fluid motion or by atomic diffusion processes we attempt to separate these

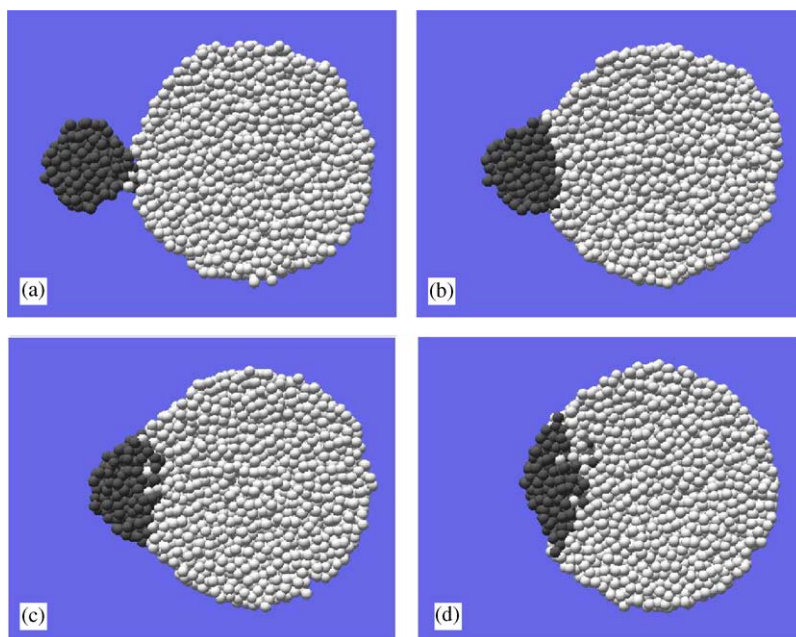


Fig. 1. Temporal snapshots of the morphology during a coalescence event for a liquid particle at 1500 K, with a volume ratio of 0.053. (a)  $t = 1$  ps, (b)  $t = 5$  ps, (c)  $t = 10$  ps, and (d)  $t = 16$  ps.

effects. Fig. 2 shows the temporal evolution of atomic velocity vectors (length of arrow is proportional to speed) in (a–d) and contour plots of the atomic speed normalized by the average speed (e–f), shown as a cross-section slice of thickness  $-0.5 \text{ nm} < y < 0.5 \text{ nm}$ , during a coalescence event for a liquid particle at 1500 K with a volume ratio of 0.053. At the initial approach, the smaller particle is accelerated toward the near stationary larger particle, as evidenced by the large magnitude (e) and similar direction to all velocity vectors (a) and results from the short range attractive forces. By contrast the velocity vectors in the larger particle are smaller and are in random directions (a,e). Even just after the collision, convection processes in the smaller particle seem to dominate the coalescence process (b). Moreover, kinetic energy in the larger particle is transferred to the smaller particle, as evidenced by the color shading differences between the smaller and larger particle (f). The reader is reminded that the simulation was conducted under a constant temperature constraint, such that the total kinetic energy of the system is invariant. However, momentum differences accelerate and deform the smaller particle during the collision. The convection processes, in addition to the kinetic energy transformation on the smaller particle, also deforms the smaller particle, as the particle seeks to spread out to make room for the atoms being convected from the trailing end of the smaller particle (c,g). The convection process decays toward the end of the coalescence process and the local deformation observed in the smaller particle is spread over the entire particle (d, h). Note that this convection process is not included in the analysis in the coalescence models (2) and (3).

A coalescence event of unequal sized near solid-like particles at 1000 K, with the volume ratio of 0.053 is shown in Fig. 3. As with the liquid case, the initial approach results in acceleration of the smaller particle (a,e). However, in the case at 1000 K, convection disappears right after the collision (b,f). Once the collision event has progressed, it is diffusion processes which drive the agglomerate to become a sphere, and the diffusion process is spread out entire particle unlike the liquid case (c,d,g,h). Fig. 4 demonstrates a coalescence event of unequal sized particles at 1000 K with the volume ratio of 0.25. At the initial approach, since the difference in particle size is not as great as the previous case, both particles are accelerated toward each other (a,e). Like the smaller volume ratio case (in Fig. 3) the convection effect disappears after the collision, and diffusion processes drive the agglomerate to become a sphere (b,f). However, towards the end of the coalescence process, atom movement in what might be termed the core of the larger particle, is seen to be amplified (c,g). Since the particle sizes in this simulation are not as significantly different from each other, the larger particle must also deform in order to evolve a spherical shape (d,h). Finally, unlike liquid particles, no internal convection can occur and the directed velocity vectors are scrambled at impact. Diffusion processes dominates the coalescence of near solid-like particles during the entire processes.

The shape and coalescence evolution is most easily quantified and tracked by calculating the temporal variation of the reduced moment of inertia, defined as the ratio of the moment of inertia in the direction normal to the collision, and the direction of the collision, as shown in Fig. 5. Here,  $x$  is the initial volume ratio of the smaller to the larger particle, where  $0 < x \leq 1$ . The total number of silicon atoms is kept constant for all cases at 10 000, with initial volume ratios, of 0.053, 0.111, 0.250, 0.429, and 1. For the calculations presented in Fig. 5, the temperature was held at 1500 K (i.e. liquid). The reduced moment of inertia converges to unity when the particle is spherical. However as these particles (1–8 nm) are dynamic, due to the atomic motion, they would never become perfectly spherical. Therefore, we define a reduced moment of inertia of 1.1 as the condition for achieving complete coalescence. From the figure one sees that the reduced moment of inertia converges to 1.1 (spherical shape) monotonically. A direct observation of all curves shows that the decay rate toward spherical shape is monotonic and decreases with increasing initial volume ratio. Moreover, the coalescence process is faster when the initial volume ratio is smaller

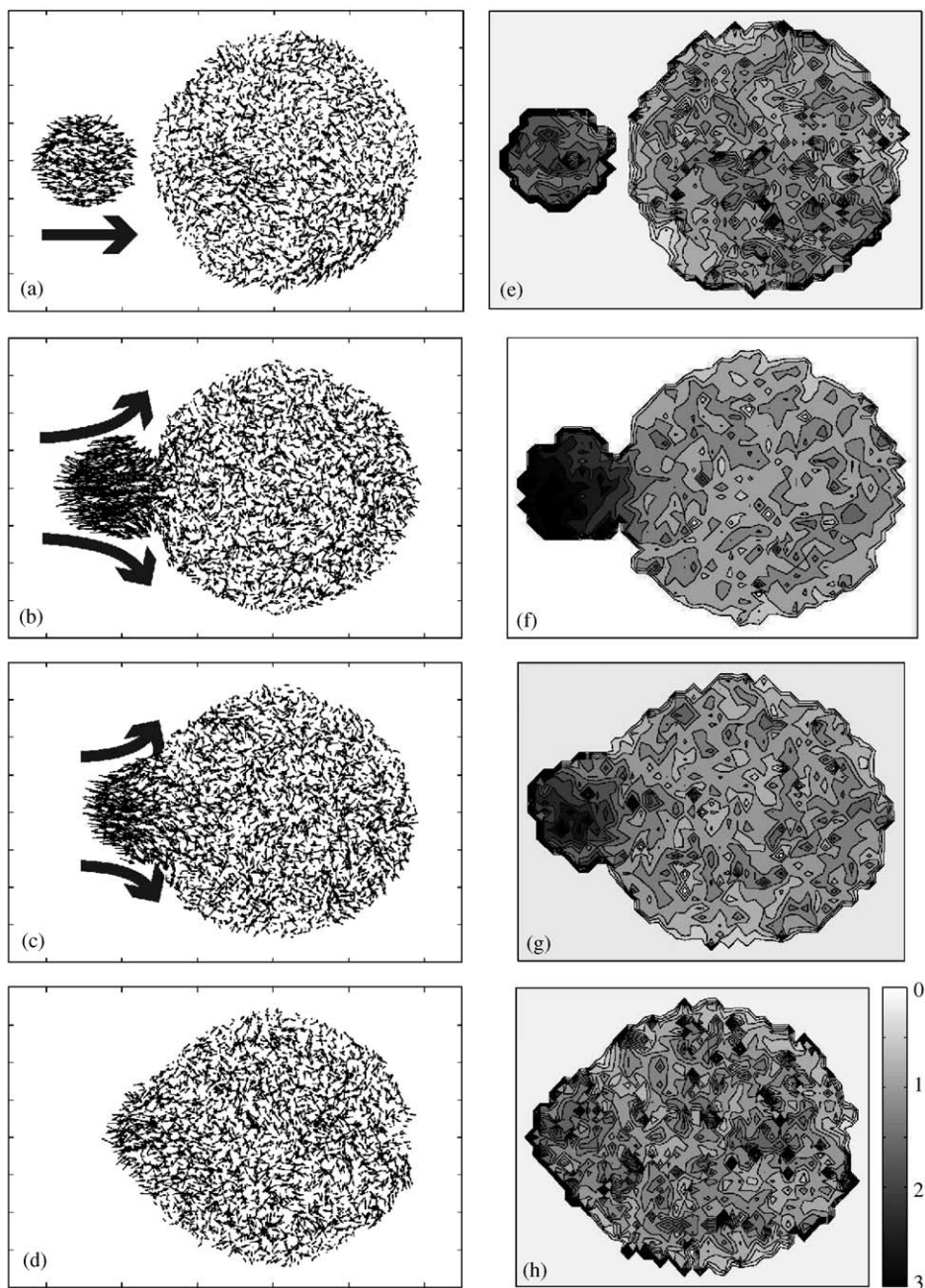


Fig. 2. Temporal evolution of atomic velocity vectors (a–d) and contour plots of the speed (e–h) shown as a cross-section slice of thickness  $-0.5 \text{ nm} < y < 0.5 \text{ nm}$ , during a coalescence event for a liquid particle at 1500 K, with a volume ratio of 0.053. (a,e)  $t = 0$  ps, (b,f)  $t = 1$  ps, (c,g)  $t = 5$  ps, and (d,h)  $t = 11$  ps.

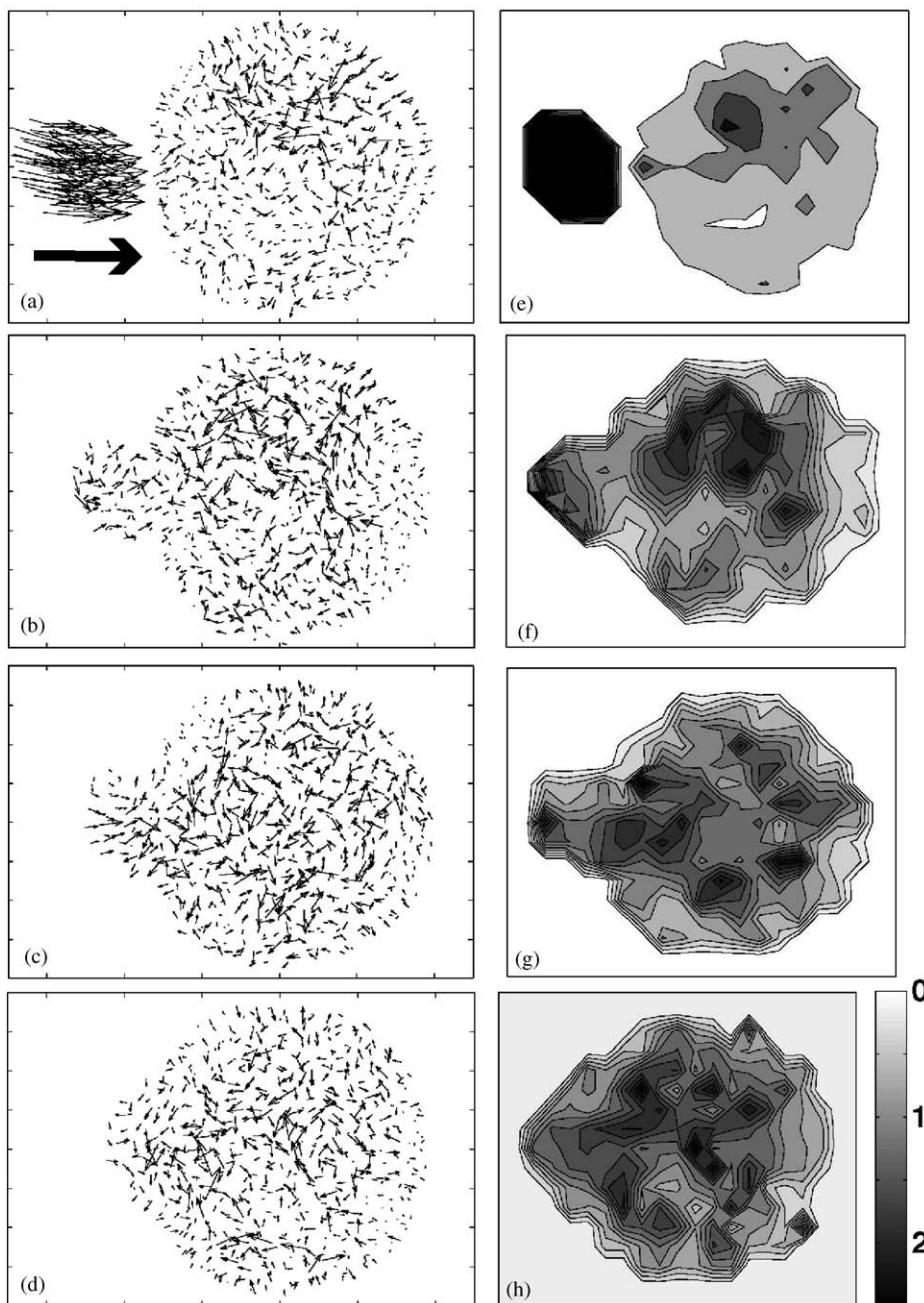


Fig. 3. Temporal evolution of atomic velocity vectors (a–d) and contour plots of the speed (e–h) shown as a cross-section slice of thickness  $-0.5 \text{ nm} < y < 0.5 \text{ nm}$ , during a coalescence event for a solid particle at 1000 K, with a volume ratio of 0.053. (a,e)  $t = 0 \text{ ps}$ , (b,f)  $t = 30 \text{ ps}$ , (c,g)  $t = 90 \text{ ps}$ , and (d,h)  $t = 140 \text{ ps}$ .

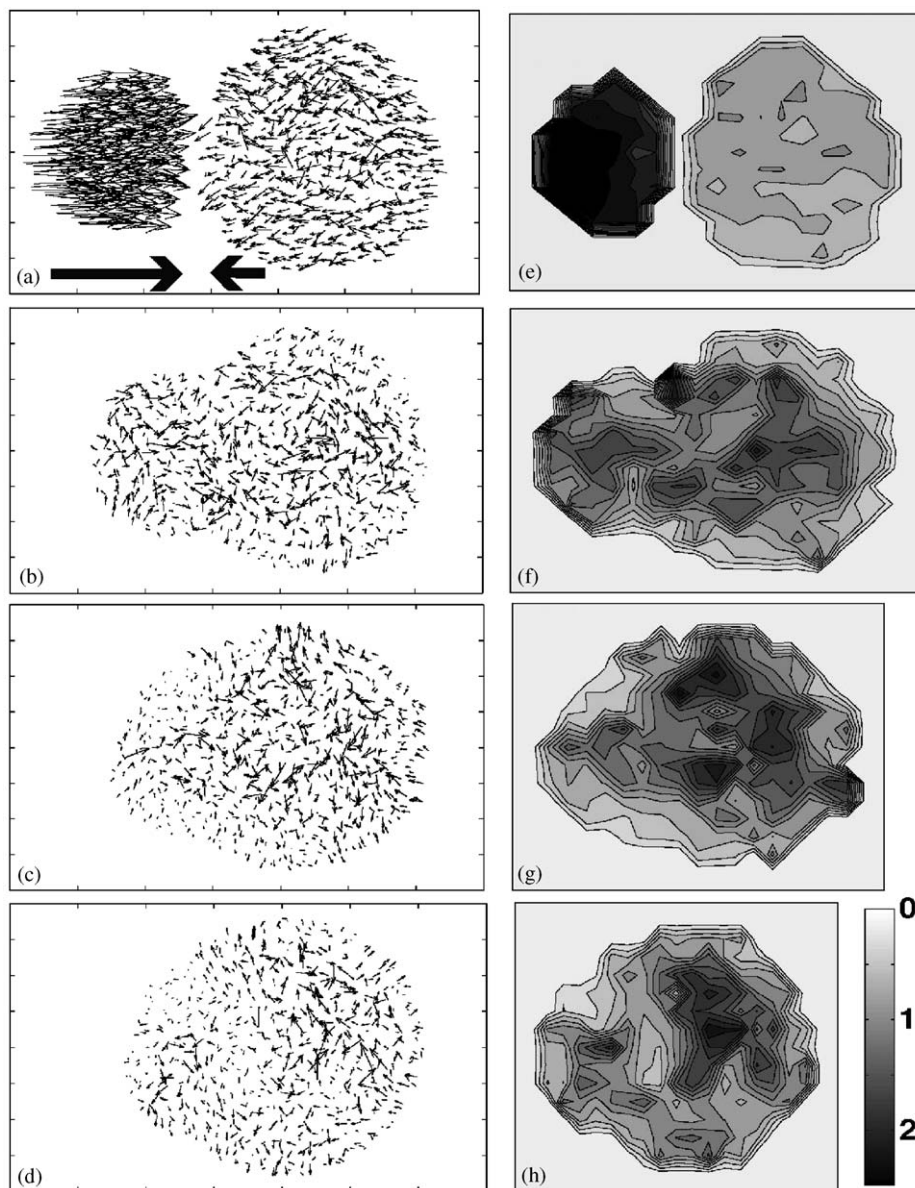


Fig. 4. Temporal evolution of atomic velocity vectors (a–d) and contour plots of the speed (e–h) shown as a cross-section slice of thickness  $-0.5 \text{ nm} < y < 0.5 \text{ nm}$ , during a coalescence event for a solid particle at 1000 K, with a volume ratio of 0.25. (a,e)  $t = 0 \text{ ps}$ , (b,f)  $t = 50 \text{ ps}$ , (c,g)  $t = 200 \text{ ps}$ , and (d,h)  $t = 300 \text{ ps}$ .

(i.e., smaller + larger particle). Since the coalescence time depends on the definition of spherical shape in terms of the reduced moment of inertia, the accuracy of the coalescence time diminishes with decreasing initial volume ratio.

Coalescence times,  $t_c$ , simulated under constant temperature processes as a function of initial particle volume ratio,  $x$ , at 1500 K (a) and 1000 K (b) shown as symbols (o) are summarized in Fig. 6. Coalescence

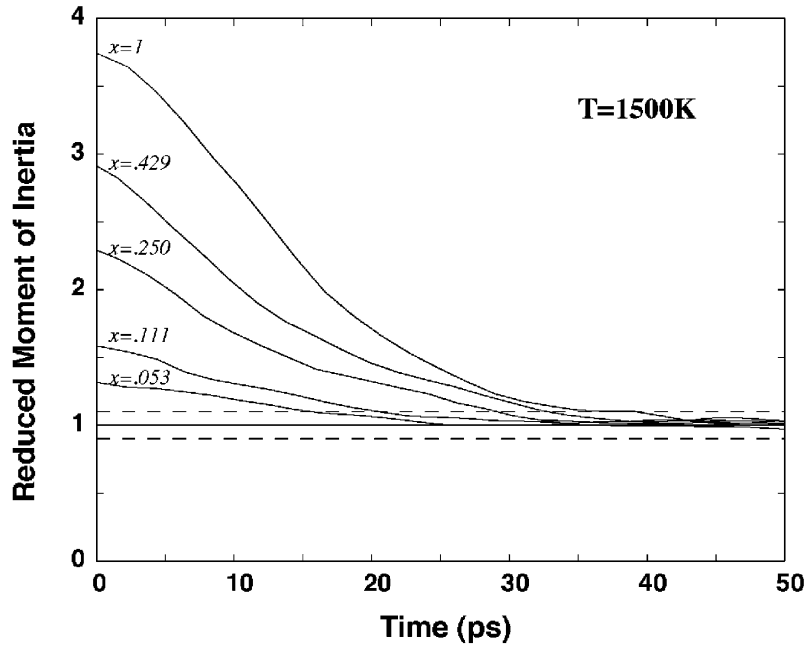


Fig. 5. Temporal behavior of the reduced moment of inertia for particles at various volume ratios. Total number of Si atoms is 10000, and the temperature is held constant at 1500 K (i.e. liquid).

times in the vertical axis in the figures are normalized by the coalescence time for two equal sized particles. At 1500 K (liquid), shown in Fig. 6(a), as the particle becomes dissimilar in size the normalized coalescence times gradually decreases. When  $x < 0.4$  the coalescence event is clearly accelerated, and when  $x \sim 0.1$ , the coalescence time has dropped to half that of the equal sized case. The normalized coalescence times obtained from the KF model (1) is shown as the solid line in the figure. Since the solution to the KF model gives an asymptotic solution, we define complete coalescence when the particle surface area,  $a$ , is  $1.05a_{\text{sph}}$ . As a result the solution presented in Figs. 6a,b are only valid for  $x < 0.025$ . The results show excellent agreement with the simulation results when  $x > 0.1$ , although significant deviation is observed for  $x = 0.05$ , which we attribute in part to the definition of complete coalescence used in the generation of the solid curve using the KF model. In general however these results indicate that the difference between the initial and final surface area dominates the coalescence kinetics of unequal sized liquid particles. Moreover, and most importantly the same characteristic coalescence time,  $\tau_f$ , may be used for any particle size ratios to obtain the coalescence time from the KF model (1). We also compare those results with the Yadha–Helble’s (YH) model, which is a numerical study of the coalescence of unequal sized droplets, shown as symbol (+) in the same figure. The YH model predicts a slightly faster coalescence time than either KF model (1) or MD results for all volume ratios. Nevertheless the trends are highly consistent.

The near solid-like particles at  $T = 1000$  K, presented in Fig. 6(b) show similar behavior to the liquid case. However, deviations between our phenomenological model and MD results become larger with decreasing initial volume ratio. The likely reason for the discrepancy is that the near solid-like particles are slow to coalesce and small effects arising from particle shape initially, the orientation of collision,

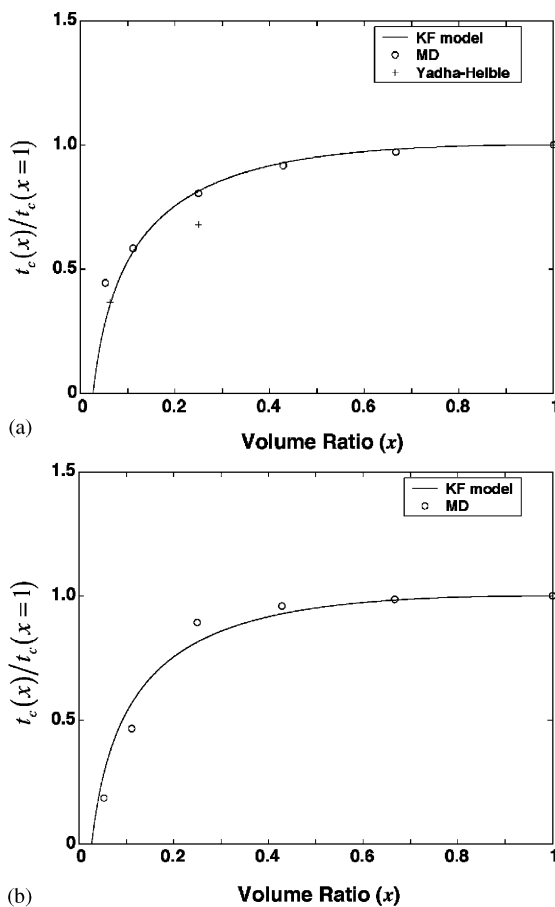


Fig. 6. Normalized coalescence times as a function of initial particle volume ratio,  $x$ . (a) 1500 K and (b) 1000 K.

etc. can change the simulated sintering time. While we believe the particles to be primarily amorphous, some short range ordering may also take place which may influence the coalescence behavior. Ideally, one would like to conduct multiple trajectories, and ensemble average the result, however at this time that is computationally not feasible. For example, the complete coalescence of one pair of equal sized particles is 48 h on Cray T3E using 8 processors.

These results indicate that the simple surface model which involves a total reduction in surface area as the driving force, regardless of initial relative particle volumes, is a reasonably sufficient and certainly, computationally tractable solution to solving for unequal particle coalescence problems.

## 5. Conclusion

Classical molecular dynamics simulations using the Stillinger–Weber potential were conducted to study the coalescence behavior of unequal sized silicon nanoparticles. The simulations were carried out over the initial particle volume ratio range of 0.053–1 with 10 000 and 1600 Si atoms at 1500 and

1000 K. It was found that the deformation of the smaller particle and convection processes dominated the coalescence of liquid nanoparticles. On the other hand, diffusion processes dominated the coalescence processes of near solid-like particles. Coalescence processes became faster when the ratio of two particle sizes (smaller/larger) approaches to zero. The Koch–Friedlander model was found capable to predict the coalescence time of two unequal sized nanoparticles, and the agreement of the model and MD results indicates that the difference between the initial and final surface area dominates the coalescence kinetics of unequal sized liquid particles.

## Acknowledgements

This work is supported by NSF Grant CTS-0083062, the Army High Performance Computing Research Center DAAD19-01-2-0014 and the Minnesota Super-Computer Center and the National Institute of Standards and Technology.

## References

- Alivisatos, A. P. (1996). Semiconductor clusters, nanocrystals, and quantum dots. *Science*, 271, 933.
- Ashgriz, N., & Poo, J. Y. (1990). Coalescence and separation in binary collisions of liquid drops. *Journal of Fluid Mechanics*, 221, 183.
- Ashgriz, N., & Poo, J. Y. (1991). Flair-flux line-segment model for advection and interface reconstruction. *Journal of Computational Physics*, 93, 449.
- Barnes, M. D., Mahurin, S. M., Mehta, A., Sumpter, B. G., & Noid, D. W. (2002). Three-dimensional photonic “molecules” from sequentially attached polymer-blend microparticles. *Physical Review Letters*, 88, 015508.
- Bolsaitis, P. P., McCarthy, J. F., & Mohiuddin, G. (1987). Formation of metal oxide aerosols for conditions of high supersaturation. *Aerosol Science and Technology*, 6, 225.
- Bradley, S. G., & Stow, C. D. (1978). Collision between liquid drops. *Philosophical Transactions of the Royal Society of London Series A*, 287, 635.
- Colvin, V. L., Alivisatos, A. P., & Tobin, J. G. (1991). Valence-band photoemission from a quantum-dot system. *Physical Review Letters*, 66, 2786.
- Foote, G. B. (1975). The water drop rebound problem dynamics of collision. *Journal of Atmospheric Research*, 32, 390.
- Frenkel, J. (1945). Viscous flow of crystalline bodies under the action of surface tension. *Journal of Physics*, 9, 385.
- Friedlander, S. K., & Wu, M. K. (1994). Linear rate law for the decay of the excess surface area of a coalescing solid particle. *Physical Review B*, 49, 3622.
- Garabedian, R. S., & Helble, J. J. (2001). A model for the viscous coalescence of amorphous particles. *Journal of Colloid and Interface Science*, 234, 248.
- Goldstein, A. N., Echer, C. M., & Alivisatos, A. P. (1992). Melting in semiconductor nanocrystals. *Science*, 256, 1425.
- Grieve, K., Mulvaney, P., & Grieser, F. (2000). Synthesis and electronic properties of semiconductor nanoparticles/quantum dots. *Current Opinion in Colloid and Interface Science*, 5, 168.
- Hawa, T., & Zachariah, M. R. (2004a). Molecular dynamics of particle–particle collisions between hydrogen–passivated silicon nanoparticles. *Physical Review B*, 69, 035417.
- Hawa, T., & Zachariah, M. R. (2004b). Internal pressure and surface tension of bare and hydrogen coated silicon nanoparticles. *Journal of Chemical Physics*, 121, 9043.
- Hawa, T., & Zachariah, M. R. (2005). Coalescence kinetics of bare and hydrogen-coated silicon nanoparticles: A molecular dynamics study. *Physical Review B*, 71, 165434.
- Helble, J. H., & Sarofim, A. F. (1989). Factors determining the primary particle size of flame-generated inorganic aerosols. *Journal of Colloid and Interface Science*, 128, 348.
- Hendy, S., Brown, S. A., & Hyslop, M. (2003). Coalescence of nanoscale metal clusters: Molecular-dynamics study. *Physical Review B*, 68, 241403.

- Jiang, Y. J., Umemura, A., & Law, C. K. (1992). An experimental investigation on the collision behaviour of hydrocarbon droplets. *Journal of Fluid Mechanics*, 234, 171.
- Koch, W., & Friedlander, S. K. (1990). The effect of particle coalescence on the surface area of a coagulating aerosol. *Journal of Colloid and Interface Science*, 140, 419.
- Kruis, F. E., Fissan, H., & Peled, A. (1998). Synthesis of nanoparticles in the gas phase for electronic, optical and magnetic applications—a review. *Journal of Aerosol Science*, 29, 511.
- Lehtinen, K. E. J., Windeler, R. S., & Friedlander, S. K. (1996). Prediction of nanoparticle size and the onset of dendrite formation using the method of characteristic times. *Journal of Aerosol Science*, 27, 883.
- Lewis, L. J., Jensen, P., & Barrat, J.-L. (1997). Melting, freezing, coalescence of gold nanoclusters. *Physical Review B*, 56, 2248.
- Mackenzie, J. K., & Shuttleworth, R. (1949). A phenomenological theory of sintering. *Proceedings of the Physical Society*, 62, 833.
- Martinez-Herrera, J. I., & Derby, J. J. (1995). Viscous sintering of spherical particles via finite element analysis. *Journal of the American Ceramic Society*, 78, 645.
- Mashayek, F., Ashgriz, N., Minkowycz, W. J., & Shotorban, B. (2003). Coalescence collision of liquid drops. *International Journal of Heat and Mass Transfer*, 46, 77.
- Matijevic, E. (1985). Production of monodispersed colloidal particles. *Annual Review of Materials Science*, 15, 483.
- Matijevic, E. (1986). Monodispersed colloids: Art and science. *Langmuir*, 2, 12.
- Menchaca-Rocha, A., Huidobro, F., Martinez-Davalos, A., Michaelian, K., Perez, A., Rodriguez, V., & Carjan, N. (1997). Coalescence and fragmentation of colliding mercury drops. *Journal of Fluid Mechanics*, 346, 291.
- Mukherjee, D., Sonwane, C. G., & Zachariah, M. R. (2003). Kinetic Monte-Carlo simulation of the effect of coalescence energy release on the size and shape evolution of nanoparticles grown as an aerosol. *Journal of Chemical Physics*, 119, 3391.
- Murray, C. B., Kagan, C. R., & Bawendi, M. G. (2000). Synthesis and characterization of monodisperse nanocrystals and close-packed nanocrystal assemblies. *Annual Review of Materials Science*, 30, 545.
- Nobari, M. R. H., Jan, Y. J., & Tryggvason, G. (1996). Head-on collision of drops—a numerical investigation. *Physics of Fluids*, 8, 29.
- Orme, M. (1997). Experiments on droplet collisions, bounce, coalescence and disruption. *Progress in Energy and Combustion Science*, 23, 65.
- Park, J. Y., & Blair, L. M. (1975). The effect of coalescence on drop size distribution in an agitated liquid-liquid dispersion. *Chemical Engineering Science*, 30, 1057.
- Raut, J. S., Bhagat, R. B., & Fichthorn, K. A. (1998). Sintering of aluminum nanoparticles: A molecular dynamics study. *NanoStructured Materials*, 10, 837.
- Ryley, D. J., & Bennett-Cowell, B. N. (1967). The collision behaviour of steam-borne water drops. *International Journal of Mechanical Sciences*, 9, 817.
- Schweigert, I. V., Lehtinen, K. E. J., Carrier, M. J., & Zachariah, M. R. (2002). Structure and properties of silica nanoclusters at high temperatures. *Physical Review B*, 65, 235410.
- Seinfeld, J. H., & Pandis, S. N. (1998). *Atmospheric chemistry and physics—from air pollution to climate change*. New York: Wiley.
- Sherer, G. W. (1977). Sintering of low-density glasses: 1 Theory. *Journal of the American Ceramic Society*, 60, 236.
- Shi, J., Gider, S., Babcock, K., & Awschalom, D. D. (1996). Magnetic clusters in molecular beams, metals, and semiconductors. *Science*, 271, 937.
- Spengler, J. D., & Gokhale, N. R. (1973). Drop impactions. *Journal of Applied Meteorology*, 12, 316.
- Stillinger, F. H., & Weber, T. A. (1985). Computer simulation of local order in condensed phase of silicon. *Physical Review B*, 31, 5262.
- Tersoff, J. (1986). New empirical model for the structural properties of silicon. *Physical Review Letters*, 56, 632.
- Tersoff, J. (1988a). New empirical approach for the structure and energy of covalent systems. *Physical Review B*, 37, 6991.
- Tersoff, J. (1988b). Empirical interatomic potential for silicon with improved elastic properties. *Physical Review B*, 38, 9902.
- Tersoff, J. (1989). Modeling solid-state chemistry: Interatomic potential for multicomponent systems. *Physical Review B*, 39, 5566.
- Trindade, T., O'Brien, P., & Pickett, N. L. (2001). Nanocrystalline semiconductors: Synthesis, properties, and perspectives. *Chemistry of Materials*, 13, 3843.
- Ulrich, G. D. (1971). Theory of particle formation and growth in oxide synthesis flames. *Combustion Science and Technology*, 4, 47.

- Ulrich, G. D., & Riehl, J. W. (1982). Aggregation and growth of submicron oxide particles in flames. *Journal of Colloid and Interface Science*, *87*, 257.
- Verlet, L. (1967). Computer 'experiments' on classical fluids. II Equilibrium correlation functions. *Physical Review*, *159*, 98.
- Xing, Y., & Rosner, D. E. (1999). Prediction of spherule size in gas phase nanoparticle synthesis. *Journal of Nanoparticle Research*, *2*, 277.
- Yadha, V., & Helble, J. J. (2004). Modeling the coalescence of heterogenous amorphous particles. *Journal of Aerosol Science*, *35*, 665.
- Zachariah, M. R., & Carrier, M. J. (1999). Molecular dynamics computation of gas-phase nanoparticles sintering: A comparison with phenomenological models. *Journal of Aerosol Science*, *30*, 1139.
- Zachariah, M. R., Carrier, M. J., & Blaisten-Barojas, J. (1996). Properties of silicon nanoparticles: A molecular dynamics study. *The Journal of Physical Chemistry*, *100*, 14856.
- Zeng, P., Zajac, S., Clapp, P. C., & Rifkin, J. A. (1998). Nanoparticle sintering simulations. *Materials Science and Engineering A*, *252*, 301.
- Zhou, H., & Derby, J. J. (1998). Three-dimensional finite-element analysis of viscous sintering. *Journal of the American Ceramic Society*, *81*, 533.
- Zhu, H., & Averback, R. S. (1996). Sintering processes of two nanoparticles: A study of molecular-dynamics simulations. *Philosophical Magazine Letters*, *73*, 27.